

## Article

# Refractory All-Ceramic Thermal Emitter for High-Temperature Near-Field Thermophotovoltaics

Fangqi Chen <sup>1</sup>, Xiaojie Liu <sup>1</sup>, Yanpei Tian <sup>1</sup> , Jon Goldsby <sup>2</sup> and Yi Zheng <sup>1,3,\*</sup> 

<sup>1</sup> Department of Mechanical and Industrial Engineering, Northeastern University, Boston, MA 02115, USA; chen.fangq@northeastern.edu (F.C.); liu.xiaojie@northeastern.edu (X.L.); tian.yan@northeastern.edu (Y.T.)

<sup>2</sup> National Aeronautics and Space Administration Glenn Research Center, Cleveland, OH 44135, USA; jon.c.goldsby@nasa.gov

<sup>3</sup> Department of Electrical and Computer Engineering, Northeastern University, Boston, MA 02115, USA

\* Correspondence: y.zheng@northeastern.edu

**Abstract:** Thermophotovoltaics is a promising technology for heat recovery and has garnered tremendous attention in the last decades. This work theoretically evaluates the performance of a thermophotovoltaic system equipped with refractory all-ceramic selective thermal emitters made of boron carbide, silicon carbide and beryllium oxide for a high working temperature of 2000 °C, which corresponds to the external quantum efficiency of a SiC/Si tandem cell. The influence of thickness and filling ratio on the emissivity of thermal emitters over the wavelength ranging from 0.2 μm to 2.5 μm is studied. The corresponding spectral heat flux and output power are analyzed as well. For a specific configuration, the parameters for the thermophotovoltaic system are obtained, including short circuit current, open circuit voltage, fill factor, total heat flux, output power and conversion efficiency. The proposed all-ceramic thermal emitter ensures the robustness in the high-temperature working condition due to its thermal stability. The tuning of emissivity is achieved and analyzed based on distinct emitter nanostructures, and the further influence on the thermophotovoltaic system performance is deeply explored. This work sheds light on research of high-temperature thermal management and power generation.

**Keywords:** thermophotovoltaics; near-field; thermal emitter; refractory



**Citation:** Chen, F.; Liu, X.; Tian, Y.; Goldsby, J.; Zheng, Y. Refractory All-Ceramic Thermal Emitter for High-Temperature Near-Field Thermophotovoltaics. *Energies* **2022**, *15*, 1830. <https://doi.org/10.3390/en15051830>

Academic Editor: Venizelos Efthymiou

Received: 5 February 2022

Accepted: 28 February 2022

Published: 2 March 2022

**Publisher's Note:** MDPI stays neutral with regard to jurisdictional claims in published maps and institutional affiliations.



**Copyright:** © 2022 by the authors. Licensee MDPI, Basel, Switzerland. This article is an open access article distributed under the terms and conditions of the Creative Commons Attribution (CC BY) license (<https://creativecommons.org/licenses/by/4.0/>).

## 1. Introduction

Nowadays, abundant waste heat is released into the environment by increasing anthropogenic activities without a deliberate plan, leaving climate issues like urban heat islands and global warming more severe. The thermophotovoltaic (TPV) system is one of the alternatives to solve this global issue and generate electrical energy meanwhile by harvesting waste heat [1]. A typical TPV system is composed of three components: a heat source, a selective thermal emitter (or a broadband emitter with a filter) and a TPV cell [2]. The heat sources for the TPV system include the combustion of fuels, concentrated solar or nuclear energy, and industrial waste heat [1]. Compared with a solar photovoltaic (PV) system, the flexibility of converting various heat energy sources enables the TPV system to work for a longer operation time and broadens the TPV application in both micro-scale and large-scale TPV generators [3,4]. A selective thermal emitter transmits electromagnetic energy by tuning heat from sources into an emission spectrum according to the bandgap of the cell [5]. The emission spectrum should match the bandgap of the TPV cell, and the low-energy photons need to be eliminated as far as possible to avoid thermal leakage, which has a negative effect on the conversion efficiency of the system [2]. To evaluate the conversion efficiency of a TPV cell more precisely, a parameter called quantum efficiency is defined as the ratio of the collected carriers to the incident photons, and it indicates the amount of current generated for a given incident photon wavelength. As all photons of a certain energy are absorbed by the cell and the resulting carriers are collected, a unity quantum

efficiency is achieved. Moreover, the quantum efficiency is equal to zero for photons with energy lower than the cell bandgap. This step-shape curve corresponds to the ideal PV cell. For a real cell case, the quantum efficiency is reduced due to effects of recombination. There are two quantum efficiencies: internal quantum efficiency (IQE) and external quantum efficiency (EQE). The difference lies in whether the optical losses such as reflection and transmission are taken into account. EQE depicts the functionality of the p-n junction in detail. Both the reflection and absorption coefficient of the incident light are taken into account, as well as the generation and collection of minority carriers [6]. The TPV system possesses merits of mechanical stability, large power output and noiselessness, rendering it promising for abundant applications, including solar TPV systems [7,8], combustion-driven TPV generators [9,10], waste heat recovery [11,12], space applications [13,14] and thermal energy storage system [15,16].

Several parameters are utilized to evaluate the performance of a PV cell, including short circuit current, open circuit voltage and fill factor. Short circuit current  $I_{SC}$  refers to the current through the PV cell as there is no potential difference across it, and it is the largest current which can be drawn from the cell. There are several factors that can have an effect on the short circuit current, including the PV cell area, the spectrum and intensity of the incident light, the absorption and reflection of the cell. It is preferred to use current density (current per unit area) instead of current so that the effect of cell area can be neglected. The solar cell performance evaluation is commonly based on the standard AM1.5 spectrum, while for the TPV scenario, the spectrum of the incident light depends on the blackbody radiation and emissivity of the thermal emitter at specific temperature. Besides, the short circuit current rises linearly with the incident light intensity. Thus, the enhanced heat flux by near-field thermal radiation will greatly increase the short circuit current. However, the conversion efficiency is not necessarily improved since the incident power also surges. Open circuit voltage  $V_{OC}$  represents the potential difference when the current is zero, and it is the maximum voltage of a PV cell as well. However, the PV cell does not work at either the short circuit current or open circuit voltage, but somewhere in between. Fill factor (FF), in conjunction with  $I_{SC}$  and  $V_{OC}$ , determines the maximum output power as  $P = I_{SC}V_{OC}FF$ . Graphically, on the current-voltage curve of the PV cell, fill factor is shown as an area ratio between the maximum inscribed rectangle and the rectangle with area equal to  $I_{SC} \times V_{OC}$ .

In order to optimize the conversion efficiency of the TPV system, emitters with tailored spectrum are often utilized to block low-energy photons that may result in an overheating effect. Emitters are categorized into two types: broadband emitters and selective emitters. A broadband emitter has a high emissivity over a large wavelength range, and its radiative spectral heat flux is similar to that of a black body, referring it as a grey body [17]. The broadband emitters radiate more photons to the cell, and a higher output power is also obtained. However, device heating from thermalization, impaired device performance and reduced conversion efficiency would possibly occur [18]. Therefore, a tailored selective emitter is preferred, which only radiates photons within a specific wavelength range. An ideal thermal emitter has a unity emissivity over the spectrum range perfectly matched with the EQE of the TPV cell, and remains zero emissivity in the rest. On the contrary to the broadband emitter, the selective emitter exhibits higher efficiency but relatively lower output. Therefore, there exists a compromise between power and efficiency to maximize the benefit for a practical application. There are quite a few review papers about selective emitters. Tian et al. reviewed tunable radiative wavelength selectivity of nano-metamaterials in both near-field and far-field radiative heat transfer [19]. Diverse structures of metamaterials were demonstrated, including nanoparticle embedded structures, and grating and multi-layered structures. Sakakibara et al. reviewed the state-of-the-art practical emitters and presented five metrics for a comprehensive evaluation [20], which include optical performance, scalability of fabrication, high-temperature stability for a long-term usage, expense and convenience of integration within the whole system. For the most practical emitter implementation, emitters used in prototype system demonstrations are categorized

based on the structure, including bulk emitters [21,22], naturally selective emitters made of rare earth metals [23], 1D photonic crystal [24,25], 2D photonic crystal [26,27], and multi-layer stack composed of subwavelength metal and dielectric layers [28,29]. However, it is a difficult issue to satisfy all the five metrics aforementioned.

In order to match the bandgap of the TPV cell, for example, gallium antimonide (GaSb), the selective emitter needs to work at 1400 °C. Hence, there are some requirements for the materials of the emitter, such as corrosion resistance, thermal stability, and high thermal conductivity [6]. The melting temperature of the material should be high enough to withstand such a harsh environment. Ghanekar et al. studied nanoparticle embedded structures for the emitter using tungsten as the refractory material [2]. Moreover, thermal stability is essential for the emitter to work well in the selected atmosphere. While metallic emitters using tungsten or tantalum have the capacity to work at high temperature, they require special packaging such as maintenance of an inert or vacuum atmosphere, which is impractical in most TPV systems. In this regard, ceramics exhibit a good stability in oxidizing atmosphere. Due to high melting temperature and good thermal stability, ceramics are commonly used for refractory thermal emitters. A number of ceramics have been brought into consideration, including silica (SiO<sub>2</sub>), alumina (Al<sub>2</sub>O<sub>3</sub>), thoria (ThO<sub>2</sub>), zirconia (ZrO<sub>2</sub>), hafnia (HfO<sub>2</sub>), magnesia (MgO) and yttria (Y<sub>2</sub>O<sub>3</sub>) [4]. By combining two or more junctions with different absorption bands, tandem solar cells offer an effective way to harvest a broad spectrum [30–32]. In this work, a refractory selective thermal emitter based on composite ceramics is designed. Three ceramic materials, boron carbide (B<sub>4</sub>C), silicon carbide (SiC) and beryllium oxide (BeO), all have a melting temperature higher than 2300 °C and exhibit outstanding thermal stability. Thus, more study of these materials are worthwhile on TPV systems. This work calculates and evaluates the performance of a TPV system integrated with a ceramic thermal emitter and a SiC/Si tandem cell. The spectral and total heat fluxes, output power and conversion efficiency are exhibited.

## 2. Theoretical Fundamentals for Analyzing Near-Field TPVs

The expressions for near-field radiative heat fluxes are derived through the dyadic Green's function [33]. The radiative heat transfer between two planes can be calculated by

$$q = \int_0^\infty \frac{d\omega}{2\pi} [\Theta(\omega, T_1) - \Theta(\omega, T_2)] \int_0^\infty \frac{k_{\parallel} dk_{\parallel}}{2\pi} Z(\omega, k_{\parallel}) \quad (1)$$

where  $T_1$  and  $T_2$  are the temperatures of two objects.  $\Theta(\omega, T) = (\hbar\omega/2)\coth(\hbar\omega/2k_B T)$  is the energy of the harmonic oscillator.  $\int_0^\infty \frac{k_{\parallel} dk_{\parallel}}{2\pi} Z(\omega, k_{\parallel})$  represents the spectral transmissivity in radiative transfer between object 1 and 2 with gap  $d$ , where  $k_{\parallel}$  is the parallel component of wavevector and  $Z(\omega, k_{\parallel})$  is known as the energy transmission coefficient [33].

The second order effective medium theory is utilized to approximate the dielectric functions of the grating structure [34]. The prerequisite for the effective medium approximation is that the wavelength  $\lambda$  is much larger than the grating period  $\Lambda$  [35].

A theoretical model can be built for near-field thermal radiation and carrier transport in PV cell by considering charge density distribution based on how photons are absorbed along the depth of the PV cell [36]. An assumption is raised that in both far-field and near-field regime, a PV cell's quantum efficiency would be the same. Thus, the calculation of the short circuit current is performed as [36]

$$I_{SC} = \int_{E_g/\hbar}^\infty \frac{e}{\hbar\omega} \cdot EQE(\omega) \cdot \frac{dq}{d\omega} d\omega \quad (2)$$

where  $E_g$  and EQE are the bandgap and the external quantum efficiency of the PV cell, respectively.  $dq/d\omega$  is the spectral heat flux, and  $e$  is the elementary charge. The dark

current  $I_0$  of the SiC/Si cell is assumed to be  $10^{-4}$  A  $m^{-2}$  based on the reference [37]. Open circuit voltage is obtained by

$$V_{OC} = (k_B T_{PV} / e) \ln(I_{SC} / I_0 + 1) \quad (3)$$

Output power of the PV cell is obtained by

$$P = I_{SC} V_{OC} FF \quad (4)$$

where FF is the fill factor which is defined by

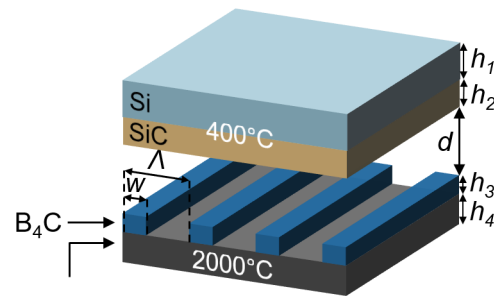
$$FF = \left[ 1 - \frac{1}{\ln(I_{SC} / I_0)} \right] \left\{ 1 - \frac{\ln[\ln(I_{SC} / I_0)]}{\ln(I_{SC} / I_0)} \right\} \quad (5)$$

The conversion efficiency of the TPV system is calculated by

$$\eta = P / q \quad (6)$$

### 3. Results and Discussion

The near-field TPV system consists of a heat source, a high-temperature thermal emitter and a PV cell, separated by a distance  $d$  smaller than the characteristic thermal wavelengths of the radiative heat transfer. As shown in Figure 1, the thermal emitter is composed of  $B_4C$  gratings and  $B_4C$ , SiC, or BeO substrate, which is referred to as Case 1, 2 and 3, respectively. The grating period  $\Lambda$  equals 50 nm and the grating width  $w$  is 10 nm, with the filling ratio equal to 0.2. The heights of the gratings,  $h_3$ , and the substrate,  $h_4$ , are both set as 50 nm. The PV cell is a SiC/Si tandem cell with 2  $\mu m$  SiC deposited on the 200  $\mu m$  Si substrate. In this work, the emitter temperature is kept at 2000  $^{\circ}C$ , while the PV cell works at 400  $^{\circ}C$ . The high-temperature operation of the PV cell is of interest to space and concentrator systems [38]. The separation distance  $d$  is fixed at 100 nm, which is much smaller than the peak thermal wavelength at 2000  $^{\circ}C$  (1.27  $\mu m$ ).



Case 1:  $B_4C$  2: SiC 3: BeO

**Figure 1.** Schematic of the near-field TPV system, consisting of a refractory selective thermal emitter and a SiC/Si tandem cell. The thermal emitter consists of  $B_4C$  gratings with three different substrates:  $B_4C$  (Case 1), SiC (Case 2) and BeO (Case 3). The grating period  $\Lambda$  and the width  $w$  are 50 nm and 10 nm, respectively. The temperature of the thermal emitter is maintained at 2000  $^{\circ}C$ , while the PV cell works at 400  $^{\circ}C$ . The separation gap  $d$  is kept as 100 nm, and the thicknesses of each layer are as follows:  $h_1 = 200$   $\mu m$ ,  $h_2 = 2$   $\mu m$ ,  $h_3 = 50$  nm and  $h_4 = 50$  nm.

The dielectric function  $\epsilon(\lambda)$  determines the emissivity spectrum of the material, thus further influencing the radiative spectral heat flux. There is a relationship between the dielectric function ( $\epsilon$ ) and the complex refractive index ( $n + i\kappa$ ):  $\sqrt{\epsilon} = n + i\kappa$ . Thus,  $n$  and  $\kappa$  are wavelength-dependent. Figure 2 demonstrates  $n$  and  $\kappa$  of the three materials involved in the thermal emitter. From Figure 2a, both the refractive indices of SiC and BeO almost remain constant from 0.44  $\mu m$  to 4  $\mu m$ . The extinction coefficient ( $\kappa$ ) of SiC exhibits an increasing trend below 1  $\mu m$ , while it is negligible through the remaining wavelength

regions.  $\kappa$  indicates the amount of attenuation when the electromagnetic wave propagates through the material, contributing to a higher absorption. Similar  $n$  and  $\kappa$  characteristics are shown in Figure 2b. For the  $B_4C$  thin film,  $n$  is quite stable above 3, while  $\kappa$  increases at shorter wavelength. Transverse electric (TE) polarization and transverse magnetic (TM) polarization are characterized by its electric field or magnetic field being perpendicular to the plane of incidence, respectively. As considering the  $B_4C$  grating structure with filling ratio of 0.2, for TE polarization, both  $n$  and  $\kappa$  values are reduced though the variation trend remains. For TM polarization,  $\kappa$  is close to zero at all wavelengths. Due to Kirchhoff's law of thermal radiation, absorptivity is equal to emissivity at thermal equilibrium state. Therefore, the increasing trend of  $\kappa$  at shorter wavelength makes a desirable selective thermal emitter for the TPV system.

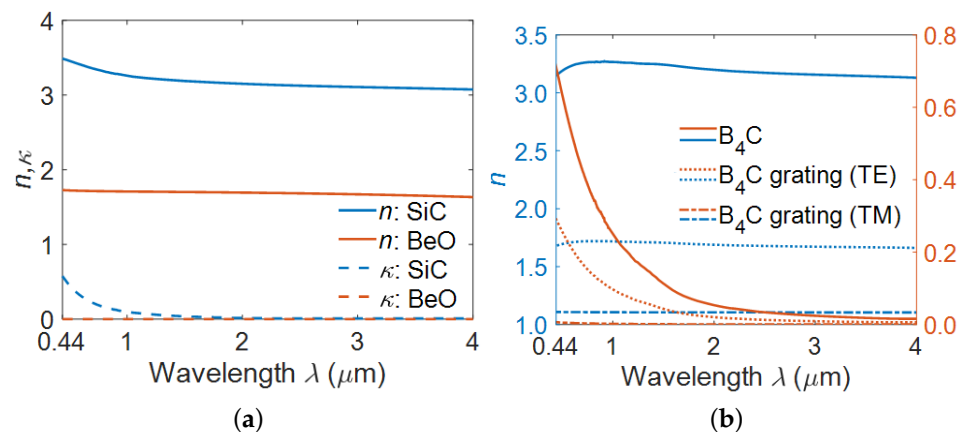


**Figure 2.** (a) Refractive indices ( $n$ ) and extinction coefficients ( $\kappa$ ) of SiC and BeO. (b) Refractive indices ( $n$ ) and extinction coefficients ( $\kappa$ ) of  $B_4C$  and  $B_4C$  grating with filling ratio of 0.2, including TE and TM polarizations.

In Figure 3, three geometric scenarios with different thicknesses and filling ratios are proposed, in each of which all the three cases are studied. The emissivity spectra with detailed parameters are shown in Figure 3a. The yellow dashed curves show the EQE of the SiC/Si cell [39]. The EQE rises steeply above the bandgap, which means it can generate electric current only when incident photons have higher energies than the bandgap of the semiconductor material. On the other side, the EQE is zero below the bandgap, thus low-energy incident photons is undesirable as it leads to thermal leakage and reduces the conversion efficiency. For the SiC/Si cell in this study, the bandgap wavelength is around 1  $\mu\text{m}$ . A desirable thermal emitter should possess emissivity matched with EQE. It can be observed from Figure 3a that a  $B_4C$  grating structure with a small filling ratio of 0.2 helps to enhance the maximum emissivity at short wavelength from around 0.7 to 0.9. Besides, as increasing the thickness from 50 nm to 100 nm, the wavelength-selective feature tends to be weakened, which means the slope becomes smaller. This increases the emissivity in the region of zero EQE, thus it may cause more thermal leakage and deteriorate the cell performance. In all the three scenarios, Case 1 and Case 2 have similar emissivity spectra, and the difference is that the emissivity of Case 2 is even lower than that of Case 1 in the region of zero EQE, which helps increase the conversion efficiency. The emissivity of Case 3 is lower and it also decreases at a shorter wavelength than Case 1 and 2. To sum up, for Case 1 and 2, scenario 1 and 3 show better match in the non-zero EQE region, while the latter two scenarios are more desirable as the wavelength exceeds 1  $\mu\text{m}$ . Regarding Case 3, scenario 3 exhibits higher emissivity than the other two scenarios in the region of zero EQE, which could impair the conversion efficiency.

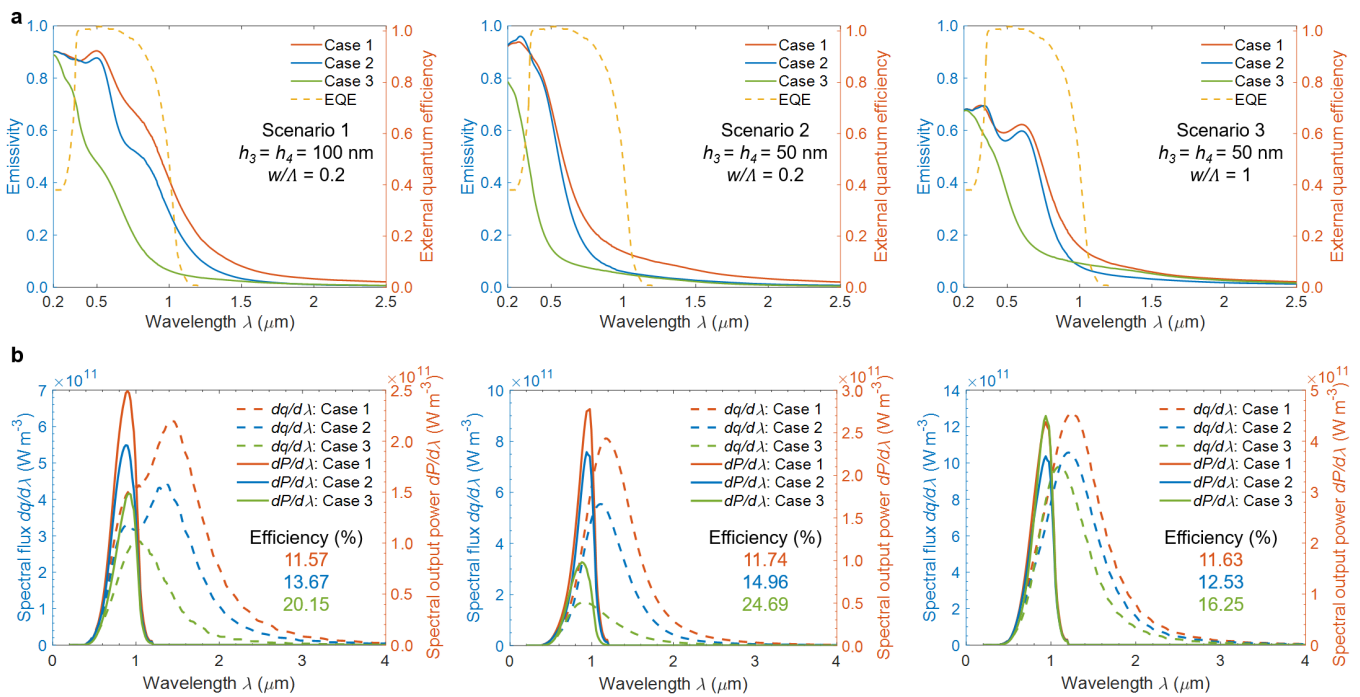


**Figure 3.** (a) Emissivity of the three thermal emitter cases. The yellow dashed line represents the EQE of the SiC/Si cell. (b) Spectral heat fluxes (dashed lines) as the separation gap is 100 nm and the corresponding spectral output power (solid lines) from the PV cell. From left to right, the two figures in each column correspond to scenario 1, 2 and 3, respectively. Case 1:  $\text{B}_4\text{C}/\text{B}_4\text{C}$ , Case 2:  $\text{B}_4\text{C}/\text{SiC}$ , and Case 3:  $\text{B}_4\text{C}/\text{BeO}$ .

Though the close match between the emissivity of the thermal emitter and the EQE of the PV cell is vital to guarantee high conversion efficiency, we also need to pay attention to the actual spectral radiative heat flux. Figure 3b shows the spectral heat flux and the corresponding spectral output power. Each figure corresponds to the upper emissivity spectra for the same scenario. It can be observed that a large portion of the spectral heat flux still lies at a wavelength larger than 1  $\mu\text{m}$ , where the EQE of the PV cell is zero. A higher emitter temperature than the present one (2000  $^\circ\text{C}$ ) is required to further move the spectral heat flux to the shorter wavelength, yet 2000  $^\circ\text{C}$  is quite close to the melting temperature of  $\text{B}_4\text{C}$  (2350  $^\circ\text{C}$ ), SiC (2730  $^\circ\text{C}$ ) and BeO (2578  $^\circ\text{C}$ ), therefore there is not much room to adjust.

Based on all the three scenarios, the  $\text{B}_4\text{C}/\text{B}_4\text{C}$  thermal emitter (Case 1) exhibits the highest heat flux, while that of the  $\text{B}_4\text{C}/\text{BeO}$  emitter (Case 3) is the lowest. The output power of Case 3 is also the lowest except in scenario 3, in which the heat flux of Case 3 is also enhanced. Instead, more long-wavelength photons lead to the lowest conversion efficiency of Case 3 ( $\eta = 16.25\%$ ) among the three scenarios. Besides, there is an obvious blue shift for the spectral heat flux for Case 3 compared with Cases 1 and 2, and this is due to the similar phenomenon observed in the emissivity spectra. Scenario 2 shows the best performance in weakening the thermal leakage effect, thus exhibiting the highest efficiency among all three cases. There exists a question regarding selective emissivity characteristics: whether we should prioritize high in-band (energy greater than bandgap) emissivity, even if the out-of-band (energy lower than bandgap) emissivity is moderately high, or ensure low out-of-band emissivity while sacrificing high in-band emissivity? Based on all the cases and scenarios discussed here, in the near-field regime, reducing the out-of-band emissivity has higher priority. This question deserves further study in both far-field and near-field TPV systems.

Detailed parameters of the TPV system (scenario 2) are displayed in Table 1 based on the calculation expressions in Section 2, including short circuit current  $I_{SC}$ , open circuit voltage  $V_{OC}$ , fill factor (FF), total heat flux  $q$ , output power  $P$  and conversion efficiency  $\eta$ . The output

power of the three cases are  $7.45 \times 10^4 \text{ W m}^{-2}$ ,  $5.95 \times 10^4 \text{ W m}^{-2}$  and  $3.19 \times 10^4 \text{ W m}^{-2}$ , while the conversion efficiencies are 11.74%, 14.96% and 24.69%, respectively. Case 1 has the highest power output but the lowest efficiency. However, the situation for Case 3 is totally reversed, with lowest power output and highest efficiency. Hence, high power output and efficiency are not achieved simultaneously for our design.

**Table 1.** Parameters for the TPV system based on scenario 2 ( $h_3 = h_4 = 50 \text{ nm}$ ,  $w/\Lambda = 0.2$ ), including short circuit current  $I_{SC}$ , open circuit voltage  $V_{OC}$ , fill factor (FF), total heat flux  $q$ , output power  $P$  and conversion efficiency  $\eta$ . The separation gap is 100 nm.

Emitter	$I_{SC}$ ( $\text{A m}^{-2}$ , $\times 10^4$ )	$V_{OC}$ (V)	FF (%)	$q$ ( $\text{W m}^{-2}$ , $\times 10^5$ )	$P$ ( $\text{W m}^{-2}$ , $\times 10^4$ )	$\eta$ (%)
Case 1 ( $\text{B}_4\text{C}/\text{B}_4\text{C}$ )	7.74	1.19	81.08	6.34	7.45	11.74
Case 2 ( $\text{B}_4\text{C}/\text{SiC}$ )	6.26	1.17	80.94	3.97	5.95	14.96
Case 3 ( $\text{B}_4\text{C}/\text{BeO}$ )	3.47	1.14	80.54	1.29	3.19	24.69

The radiative heat transfer and the TPV performance are also studied at various separation gaps even in the far-field ( $d > 1000 \text{ nm}$ ) in Figure 4. These results are based on scenario 2. Figure 4a displays the total heat fluxes and output power against the separation gap from 10 nm to 10  $\mu\text{m}$ . Obviously, the heat fluxes rise monotonically with a smaller separation gap, and this is due to the coupling of surface waves in the near-field thermal radiation. Consequently, the total output power increases as well. In the far-field regime ( $d > 1000 \text{ nm}$ ), the heat fluxes and power are essentially independent of the gap. From Figure 4b, it is observed that at the gap of 100 nm, Case 3 has higher conversion efficiency than Case 1 and 2, while the heat flux of Case 3 is the lowest (Figure 4a). This is due to increased selectivity of high-energy photons, resulting in lower losses for Case 3. In Figure 3b, Scenario 2, it is shown that for Case 1 and 2, a large part of the spectral heat fluxes are in the zero EQE region, and these heat fluxes cannot be converted into electricity and are wasted instead, which leads to lower conversion efficiency. Besides, the oscillatory behavior of efficiency can be explained by vacuum gap behaving like a waveguide, and similar phenomenon has been reported in the previous work [40]. Besides, though the near-field regime can enhance the radiative heat flux and the output power as well, the improvement of the conversion efficiency is not obvious and may even be reduced compared with the far-field regime.

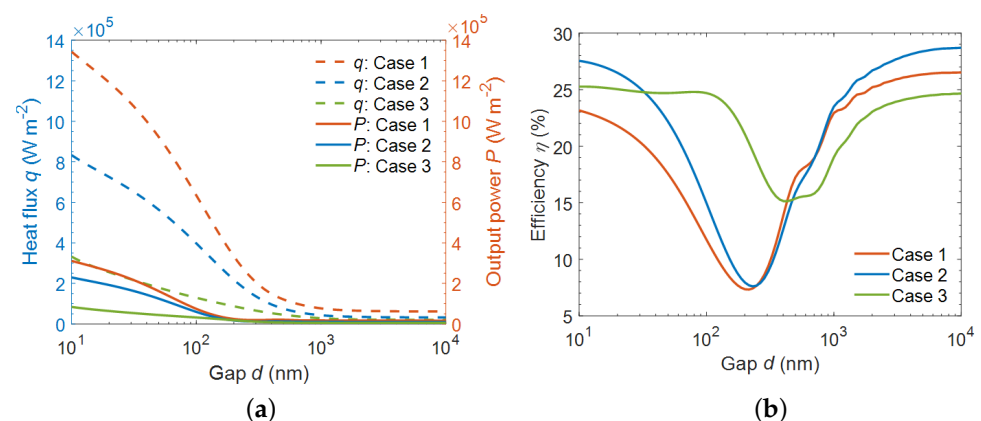


**Figure 4.** (a) Total heat fluxes (dashed lines) and output power (solid lines) as a function of the separation gap. (b) Variation in conversion efficiency against the separation gap. These results are based on scenario 2.

#### 4. Conclusions

In summary, this work proposes refractory selective thermal emitters based on composite ceramics and theoretically analyzes their performance in a near-field TPV system. The selective emitter and the SiC/Si cell work at 2000  $^\circ\text{C}$  and 400  $^\circ\text{C}$ , respectively, and are

separated by a nanoscale gap of 100 nm. Three geometric scenarios with different thicknesses and filling ratios have been studied to understand the influence on the emissivity spectra. To obtain a high conversion efficiency, the emissivity spectra and the corresponding spectral heat fluxes are studied. Regarding the selective thermal emitter, there exists a balance between high in-band emissivity and low out-of-band emissivity for the purpose of high conversion efficiency. Based on this work, reducing the out-of-band emissivity has higher priority. For the proposed configuration (scenario 2), the conversion efficiencies for each case ( $B_4C/B_4C$ ,  $B_4C/SiC$ , and  $B_4C/BeO$ ) reach 11.74%, 14.96% and 24.69%, respectively. Moreover, compared with far-field emitter systems, the near-field TPV will enhance the output power, yet higher efficiency is not guaranteed. This work designs a refractory ceramics-based selective thermal emitter and elaborates the performance in a TPV system, shedding light on research of high-temperature thermal management, energy harvesting and power generation.

**Author Contributions:** Conceptualization, F.C. and Y.Z.; methodology, F.C.; validation, F.C., X.L. and Y.T.; formal analysis, F.C.; writing—original draft preparation, F.C.; writing—review and editing, F.C., J.G. and Y.Z.; visualization, F.C.; supervision, Y.Z.; funding acquisition, Y.Z. All authors have read and agreed to the published version of the manuscript.

**Funding:** This research was funded by the National Science Foundation through grant number CBET-1941743 and NASA Glenn Faculty Fellowship Program.

**Data Availability Statement:** The data that support the findings of this study are available from the corresponding author upon reasonable request.

**Conflicts of Interest:** The authors declare no conflict of interest.

## References

1. Gamel, M.M.A.; Lee, H.J.; Rashid, W.E.S.W.A.; Ker, P.J.; Yau, L.K.; Hannan, M.A.; Jamaludin, M. A Review on Thermophotovoltaic Cell and Its Applications in Energy Conversion: Issues and Recommendations. *Materials* **2021**, *14*, 4944. [[CrossRef](#)] [[PubMed](#)]
2. Ghanekar, A.; Lin, L.; Zheng, Y. Novel and efficient Mie-metamaterial thermal emitter for thermophotovoltaic systems. *Optics Express* **2016**, *24*, A868–A877. [[CrossRef](#)] [[PubMed](#)]
3. Basu, S.; Chen, Y.B.; Zhang, Z. Microscale radiation in thermophotovoltaic devices—A review. *Int. J. Energy Res.* **2007**, *31*, 689–716. [[CrossRef](#)]
4. Bauer, T. *Thermophotovoltaics: Basic Principles and Critical Aspects of System Design*; Springer: Berlin/Heidelberg, Germany, 2011.
5. Chen, Z.; Adair, P.L.; Rose, M. Investigation of energy conversion in TPV power generation prototype using blackbody/selective emitters. In Proceedings of the IECEC-97 Proceedings of the Thirty-Second Intersociety Energy Conversion Engineering Conference, Honolulu, HI, USA, 27 July–1 August 1997; Volume 2, pp. 1097–1100.
6. Ferrari, C.; Melino, F.; Pinelli, M.; Spina, P.R.; Venturini, M. Overview and status of thermophotovoltaic systems. *Energy Procedia* **2014**, *45*, 160–169. [[CrossRef](#)]
7. Zhou, Z.; Sakr, E.; Sun, Y.; Bermel, P. Solar thermophotovoltaics: Reshaping the solar spectrum. *Nanophotonics* **2016**, *5*, 1–21. [[CrossRef](#)]
8. Xuan, Y.; Chen, X.; Han, Y. Design and analysis of solar thermophotovoltaic systems. *Renew. Energy* **2011**, *36*, 374–387. [[CrossRef](#)]
9. De Pascale, A.; Ferrari, C.; Melino, F.; Morini, M.; Pinelli, M. Integration between a thermophotovoltaic generator and an Organic Rankine Cycle. *Appl. Energy* **2012**, *97*, 695–703. [[CrossRef](#)]
10. Chan, W.R.; Stelmakh, V.; Waits, C.M.; Soljacic, M.; Joannopoulos, J.D.; Celanovic, I. Photonic Crystal Enabled Thermophotovoltaics for a Portable Microgenerator. *J. Phys. Conf. Ser.* **2015**, *660*, 012069. [[CrossRef](#)]
11. Utlu, Z.; Parali, U. Investigation of the potential of thermophotovoltaic heat recovery for the Turkish industrial sector. *Energy Convers. Manag.* **2013**, *74*, 308–322. [[CrossRef](#)]
12. Bauer, T.; Forbes, I.; Pearsall, N. The potential of thermophotovoltaic heat recovery for the UK industry. *Int. J. Ambient. Energy* **2004**, *25*, 19–25. [[CrossRef](#)]
13. Datas, A.; Martí, A. Thermophotovoltaic energy in space applications: Review and future potential. *Solar Energy Mater. Sol. Cells* **2017**, *161*, 285–296. [[CrossRef](#)]
14. Wang, X.; Liang, R.; Fisher, P.; Chan, W.; Xu, J. Radioisotope thermophotovoltaic generator design methods and performance estimates for space missions. *J. Propuls. Power* **2020**, *36*, 593–603. [[CrossRef](#)]
15. Datas, A.; Ramos, A.; Martí, A.; del Cañizo, C.; Luque, A. Ultra high temperature latent heat energy storage and thermophotovoltaic energy conversion. *Energy* **2016**, *107*, 542–549. [[CrossRef](#)]
16. Amy, C.; Seyf, H.R.; Steiner, M.A.; Friedman, D.J.; Henry, A. Thermal energy grid storage using multi-junction photovoltaics. *Energy Environ. Sci.* **2019**, *12*, 334–343. [[CrossRef](#)]

17. Chubb, D. *Fundamentals of Thermophotovoltaic Energy Conversion*; Elsevier: Amsterdam, The Netherlands, 2007.
18. DeMeo, D.F.; Licht, A.S.; Shemelya, C.M.; Downs, C.M.; Vandervelde, T.E. Thermophotovoltaics: An alternative to and potential partner with rectenna energy harvesters. In *Rectenna Solar Cells*; Springer: Berlin/Heidelberg, Germany, 2013; pp. 371–390.
19. Tian, Y.; Ghanekar, A.; Ricci, M.; Hyde, M.; Gregory, O.; Zheng, Y. A review of tunable wavelength selectivity of metamaterials in near-field and far-field radiative thermal transport. *Materials* **2018**, *11*, 862. [[CrossRef](#)]
20. Sakakibara, R.; Stelmakh, V.; Chan, W.R.; Ghebrebrhan, M.; Joannopoulos, J.D.; Soljacic, M.; Čelanović, I. Practical emitters for thermophotovoltaics: A review. *J. Photonics Energy* **2019**, *9*, 032713. [[CrossRef](#)]
21. Nielsen, O.M.; Arana, L.R.; Baertsch, C.D.; Jensen, K.F.; Schmidt, M.A. A thermophotovoltaic micro-generator for portable power applications. In Proceedings of the 12th International Conference on Solid-State Sensors, Actuators and Microsystems, Boston, MA, USA, 9–12 June 2003; Volume 1, pp. 714–717.
22. Fraas, L.; Samaras, J.; Avery, J.; Minkin, L. Antireflection coated refractory metal matched emitters for use with GaSb thermophotovoltaic generators. In Proceedings of the Conference Record of the Twenty-Eighth IEEE Photovoltaic Specialists Conference-2000, Anchorage, AK, USA, 15–22 September 2000; pp. 1020–1023.
23. Bitnar, B.; Durisch, W.; Mayor, J.C.; Sigg, H.; Tschudi, H. Characterisation of rare earth selective emitters for thermophotovoltaic applications. *Sol. Energy Mater. Sol. Cells* **2002**, *73*, 221–234. [[CrossRef](#)]
24. Bierman, D.M.; Lenert, A.; Chan, W.R.; Bhatia, B.; Čelanović, I.; Soljačić, M.; Wang, E.N. Enhanced photovoltaic energy conversion using thermally based spectral shaping. *Nat. Energy* **2016**, *1*, 16068. [[CrossRef](#)]
25. Lenert, A.; Bierman, D.M.; Nam, Y.; Chan, W.R.; Čelanović, I.; Soljačić, M.; Wang, E.N. A nanophotonic solar thermophotovoltaic device. *Nat. Nanotechnol.* **2014**, *9*, 126–130. [[CrossRef](#)]
26. Chan, W.R.; Stelmakh, V.; Ghebrebrhan, M.; Soljačić, M.; Joannopoulos, J.D.; Čelanović, I. Enabling efficient heat-to-electricity generation at the mesoscale. *Energy Environ. Sci.* **2017**, *10*, 1367–1371. [[CrossRef](#)]
27. Rinnerbauer, V.; Lenert, A.; Bierman, D.M.; Yeng, Y.X.; Chan, W.R.; Geil, R.D.; Senkevich, J.J.; Joannopoulos, J.D.; Wang, E.N.; Soljačić, M.; et al. Metallic photonic crystal absorber-emitter for efficient spectral control in high-temperature solar thermophotovoltaics. *Adv. Energy Mater.* **2014**, *4*, 1400334. [[CrossRef](#)]
28. Kohiyama, A.; Shimizu, M.; Yugami, H. Unidirectional radiative heat transfer with a spectrally selective planar absorber/emitter for high-efficiency solar thermophotovoltaic systems. *Appl. Phys. Express* **2016**, *9*, 112302. [[CrossRef](#)]
29. Shimizu, M.; Kohiyama, A.; Yugami, H. High-efficiency solar-thermophotovoltaic system equipped with a monolithic planar selective absorber/emitter. *J. Photonics Energy* **2015**, *5*, 053099. [[CrossRef](#)]
30. Heidarzadeh, H.; Baghban, H.; Rasooli, H.; Dolatyari, M.; Rostami, A. A new proposal for Si tandem solar cell: Significant efficiency enhancement in 3C-SiC/Si. *Optik* **2014**, *125*, 1292–1296. [[CrossRef](#)]
31. Faisal, A.R.M.; Nguyen, T.; Dinh, T.; Nguyen, T.K.; Tanner, P.; Streed, E.W.; Dao, D.V. 3C-SiC/Si heterostructure: An excellent platform for position-sensitive detectors based on photovoltaic effect. *ACS Appl. Mater. Interfaces* **2019**, *11*, 40980–40987. [[CrossRef](#)]
32. Faisal, A.R.M.; Dinh, T.; Tanner, P.; Phan, H.P.; Nguyen, T.K.; Streed, E.W.; Dao, D.V. Photoresponse of a highly-rectifying 3C-SiC/Si heterostructure under UV and visible illuminations. *IEEE Electron Device Lett.* **2018**, *39*, 1219–1222. [[CrossRef](#)]
33. Narayanaswamy, A.; Zheng, Y. A Green's function formalism of energy and momentum transfer in fluctuational electrodynamics. *J. Quant. Spectrosc. Radiat. Transf.* **2014**, *132*, 12–21. [[CrossRef](#)]
34. Raguin, D.H.; Morris, G.M. Antireflection structured surfaces for the infrared spectral region. *Appl. Opt.* **1993**, *32*, 1154–1167. [[CrossRef](#)]
35. Chen, Y.B.; Zhang, Z.; Timans, P. Radiative Properties of Patterned Wafers with Nanoscale Linewidth. *J. Heat Transf.* **2007**, *129*, 79–90. [[CrossRef](#)]
36. Park, K.; Basu, S.; King, W.; Zhang, Z. Performance analysis of near-field thermophotovoltaic devices considering absorption distribution. *J. Quant. Spectrosc. Radiat. Transf.* **2008**, *2*, 305–316. [[CrossRef](#)]
37. Faisal, A.R.M.; Dinh, T.; Nguyen, V.T.; Tanner, P.; Phan, H.P.; Nguyen, T.K.; Haylock, B.; Streed, E.W.; Lobino, M.; Dao, D.V. Self-powered broadband (UV-NIR) photodetector based on 3C-SiC/Si heterojunction. *IEEE Trans. Electron Devices* **2019**, *66*, 1804–1809. [[CrossRef](#)]
38. Singh, P.; Ravindra, N.M. Temperature dependence of solar cell performance—an analysis. *Sol. Energy Mater. Sol. Cells* **2012**, *101*, 36–45. [[CrossRef](#)]
39. Kabe, M.D.; Lare, Y.; Ottaviani, L.; Pasquinelli, M.; Barakel, D.; Portail, M. Simulation and optimization of the nSiC layer's thickness in a nSiC/pSi photovoltaic cell. *OAJ Mater. Devices* **2019**, *4*, 1. [[CrossRef](#)]
40. Tong, J.K.; Hsu, W.C.; Huang, Y.; Boriskina, S.V.; Chen, G. Thin-film 'thermal well' emitters and absorbers for high-efficiency thermophotovoltaics. *Sci. Rep.* **2015**, *5*, 10661. [[CrossRef](#)] [[PubMed](#)]